Multiplet effects in the electronic correlation of one-dimensional magnetic transition metal oxides on metals

J. Goikoetxea,[1] C. Friedrich,[2] G. Bihlmayer,[2] S. Blügel,[2] A. Arnau,[1,3,4] and M. Blanco-Rey[3,4]

[1]*Centro de Física de Materiales CFM/MPC (CSIC-UPV/EHU), Paseo Manuel de Lardizábal 5, 20018 Donostia-San Sebastián, Spain*

[2]*Peter Grünberg Institut and Institute for Advanced Simulation, Forschungszentrum Jülich and JARA, 52425 Jülich, Germany*

[3]*Departamento de Polímeros y Materiales Avanzados: Física, Química y Tecnología, Universidad del País Vasco UPV/EHU, Apartado 1072, 20080 Donostia-San Sebastián, Spain*

[4]*Donostia International Physics Center, Paseo Manuel de Lardizábal 4, 20018 Donostia-San Sebastián, Spain*

(Received 23 February 2022; revised 8 June 2022; accepted 1 July 2022; published 19 July 2022)

We use the constrained random-phase approximation (cRPA) method to calculate the Hubbard U parameter in four one-dimensional magnetic transition metal atom oxides of composition XO_2 (X = Mn, Fe, Co, Ni) on Ir(100). In addition to the expected screening of the oxide, i.e., a significant reduction of the U value by the presence of the metal substrate, we find a strong dependence on the electronic configuration (multiplet) of the X(d) orbital. Each particular electronic configuration attained by atom X is dictated by the O ligands, as well as by the charge transfer and hybridization with the Ir(100) substrate. We find that MnO_2 and NiO_2 chains exhibit two different screening regimes, while the case of CoO_2 is somewhere in between. The electronic structure of the MnO_2 chain remains almost unchanged upon adsorption. Therefore, in this regime, the additional screening is predominantly generated by the electrons of the neighboring metal surface atoms. The screening strength for NiO_2/Ir(100) is found to depend on the Ni(d) configuration in the adsorbed state. The case of FeO_2 shows an exceptional behavior, as it is the only insulating system in the absence of the metallic substrate and, thus, it has the largest U value. However, this value is significantly reduced by the two mentioned screening effects after adsorption.

DOI: 10.1103/PhysRevB.106.035130

I. INTRODUCTION

The metallic or insulating character of a system often lies beyond the descriptive power of one-electron models. In systems with localized electrons, such as in d electrons, the existence of a gap is determined by three quantities: (i) the charge transfer (CT) gap Δ_{Ld} from a ligand (L) to the open d shell, (ii) the bandwidth that results from hybridization, and (iii) the d-orbital intrashell electron-electron Coulomb interaction, usually expressed in terms of correlation U and exchange J parameters. The renowned Zaanen-Sawatzky-Allen (ZSA) diagram abridges the various insulating and metallic phases resulting from these interactions [1]. Likewise, exchange interactions between spin-polarized ions stem from the aforementioned terms of the Hubbard Hamiltonian, as a direct consequence of the competition between electron itinerance and intrashell Coulomb interaction. While the bare interaction amounts to a few tens of eV in 3d transition metals (TM), the effective interaction is strongly damped by the electronic screening. Therefore, its magnitude depends on the electronic structure of the particular system, e.g., on the hybridization of the d orbitals and charge transfer effects. It has been found that the effective interaction parameter is of a few eV in bulk oxides and, at the metal/oxide interface, the Coulomb interaction is further screened by twice the image charge formation potential [2,3]. The dimensionality d determines the screening length: for $d \leqslant 2$, long-range screening is suppressed and antiscreening may exist at intermediate interatomic distances [4,5].

Several electronic structure methods rely on realistic effective U parameters to account for screening mechanisms as an alternative to more complex calculations. In this context, the popular LDA + U [6] used in density-functional theory (DFT) allows to include correlation effects via an orbital-dependent functional that is applied specifically to the localized orbitals. It can be formulated as a rotationally invariant functional dependent on constant U and J values [7]. In the next level of complexity we find many-body methods beyond the one-electron picture of DFT, for example, LDA++ [8], GW [9], MP2 [10], or RPA [11] and, notably, methods based on dynamical mean-field theory (DMFT) [12–14].

LDA + U and DMFT-based methods require suitable U and J parameters to predict correlation-dependent properties. A number of methods have been proposed to determine those quantities self-consistently from first principles, such as constrained DFT [15,16] (recently improved to avoid supercell calculations [17,18]) and constrained random-phase approximation (cRPA) [19,20]. The latter approach also gives access to the frequency dependence of the interaction. In it, the polarizability contribution of electrons in the correlated subspace is excluded to obtain a screened interaction $\hat{U}$, whose matrix elements in the localized basis are the sought-for $U_{mn,m'n'}$ Coulomb matrix elements of the Hubbard Hamiltonian, where indices label the orbitals. In practice, maximally

 ©2022 American Physical Society

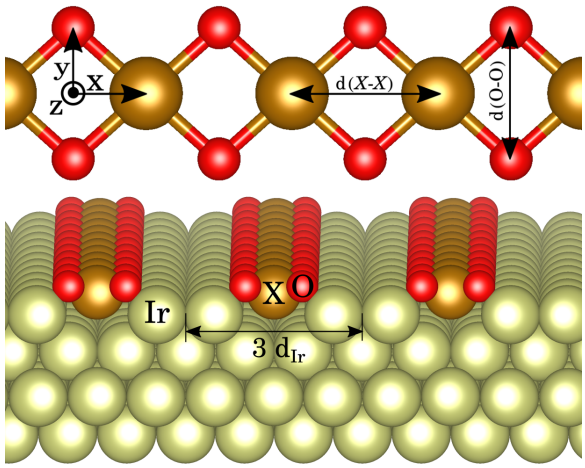

FIG. 1. Atomic structure of the free-standing (top) and adsorbed chains (bottom) on the missing-row (3 × 1) Ir(100) surface.

localized Wannier functions (MLWF) are used as basis sets [21–24].

In this paper, we use cRPA to calculate $\hat{U}$ in four one-dimensional magnetic transition-metal oxides (TMO) of composition XO_2 (X = Mn, Fe, Co, Ni) on Ir(100). In addition to the expected screening effect of the metal substrate, we find a strong dependence of the U value on the electronic configuration (multiplet) of the X(d) orbital. The particular configuration attained by X is dictated by the O ligands, as well as by the charge transfer and hybridization with the substrate. MnO_2 and NiO_2 chains represent two different regimes. The electronic structure of the MnO_2 chain remains almost unchanged upon adsorption. In this regime screening by the neighboring metal surface atoms applies. In contrast, NiO_2/Ir is in the other regime, where screening is dominated by the Ni(d) configuration adopted in the adsorbed state. The cRPA calculations show that the multiplet effect cannot be uncoupled from screening by the metal.

XO_2 chains grown in ultrahigh vacuum on Ir(100) are aligned along the [100] crystallographic direction and can reach lengths up to 130 nm [25]. The chains self-organize in a (3 × 1) missing-row superstructure (see Fig. 1) with rotational domains of ∼100 nm^2 extension. Low-energy electron diffraction [LEED-I(V)] shows that the Ir atoms below the chain are lifted to leave room for the X atoms, which are not coplanar with the oxygens [25,26]. Pt(100) can serve as growth template as well [26,27]. DFT + U calculations in the literature have used a low value $U - J = 1.5$ eV for these systems on the premise that the interactions within the X(d) orbital are heavily screened by the metal substrate [25,27]. Weak antiferromagnetic (AFM) coupling is found along MnO_2 and CoO_2 on Ir(100) [25] and CoO_2 on Rh(553) [28], FeO_2/Ir(100) is ferromagnetic (FM) and the Ni spin moment in NiO_2/Ir(100) is quenched [25]. A long-range chiral noncollinear modulation is also observed along MnO_2/Pt(100) using scanning tunneling microscopy [27]. Substrate-mediated RKKY exchange promotes additional lateral interactions between the MnO_2/Ir(100) chains, which are also noncollinear and chiral [29]. The modeling of these magnetic properties is subject to understanding Coulomb interactions. As a matter of fact, a variation in the Curie and Néel critical temperatures has been observed during magnetic oxide film growth on metals that can be explained by the image potential screening length [30,31]. As a first approximation, the magnetic exchange along the chain follows from the electron hopping through X(d)-O(p)-X(d) orbitals (superexchange) [32,33]. In the CT insulator limit ($U \gg \Delta_{pd}$) [1], the coupling constant of the AFM channel roughly scales as $\sim t^4/U^3$, where t accounts for the hopping integrals, and the FM one as $\sim -t^2/U$. Additionally, the fourfold coordination of X(d) allows for competing hopping pathways that tend to weaken the magnetic interactions [28]. All in all, the combined effect of the O(p) ligands and Ir substrate screening channels will lead to a system-dependent renormalization of intraorbital X(d) interactions with consequences for the previously described magnetic properties. This understanding of system dependent interactions is the purpose of this study.

The paper is organized as follows: In Sec. II we describe the DFT and cRPA calculations; the results and discussion are presented in Sec. III, which is divided into Secs. III A and III B on the isolated and the adsorbed chains on Ir(100), respectively. Finally, conclusions are drawn in Sec. IV.

II. THEORETICAL METHODS

Ideal free-standing planar XO_2 chains are modelled in the supercell approach in their ferromagnetic state. The geometry is found by relaxing the X-X distances and X-O bonds in a calculation with the VASP code (projector augmented wave potentials and a plane-wave basis set [34,35]) using the GGA + U approximation [25,29]. The details of the geometry determination are described in Tables S1 and S2 in the Supplemental Material (SM) [36]. For the XO_2/Ir(100) model structures, also in their ferromagnetic state, a (3 × 1) missing-row reconstructed substrate (see Fig. 1) with the experimental in-plane lattice constant $a = 2.71$ Å is used, as found in the LEED-I(V) study of Ref. [25]. The substrate slab consists of five monolayers, where the bottom layer is kept fixed during the relaxation. Two layers are kept in the cRPA calculations [37]. These geometry relaxations have been carried out at a fixed value $U = 1.5$ eV, used also in other papers with supported XO_2 chains [25,29]. In the coplanar isolated chains the equilibrium geometry shows little sensitivity to the U value, but the spin state can be altered by a change in U (see Fig. S1 in the SM [36]).

The one-electron wavefunctions used in the cRPA calculations are obtained from *ab initio* DFT + U calculations [6] with the generalized-gradient PBE functional [38] in the fully-localized limit [39] for the LDA + U double-counting term. The used code, FLEUR [40], is based on the full-potential linearized augmented plane waves (FLAPW) formalism [41–43]. The local basis functions are expanded to $l_{max} = 8, 6$ and 8 inside the X, O and Ir muffin tin spheres, of radii 2.1, 1.2 and 2.4 a.u., respectively. The wavevector cut-off in the interstitial region is 5 a.u.$^{-1}$ for wavefunctions and 14 a.u.$^{-1}$ for the potential, using a 10 × 3 × 3 Brillouin zone sampling (the sampling in the perpendicular direction is needed for constructing the Wannier functions). The Fermi level was determined by a Fermi-Dirac smearing of width 0.27 eV. To adapt these parameters to each particular case,

slight modifications are performed that can be found in Table S3 in the SM [36].

For the unsupported XO_2 chains, MLWFs [21,22] for 11 bands are constructed with projections of d type on X = Fe, Co, Ni, and s, p_x, p_z or $p = (p_x, p_y, p_z)$ orbitals on O. For MnO_2, 13 bands are needed (d on Mn and s, p on O). In the supported case, the Wannier basis needs to be extended to include the Ir states, since the oxide states are strongly hybridized with the metal substrate. Up to 41 bands are considered, including p, d projections on X, s, p on O and sp^3d on Ir. The static partially screened Coulomb interaction matrices in the Wannier basis are calculated with the cRPA formalism as implemented in the code SPEX [44], where correlated subspaces can be selected *ad hoc* to obtain information about different screening channels in the system. The effective parameters U, J are obtained by averaging the Coulomb interaction matrix elements as described in Ref. [39].

In cRPA, the Hilbert space is divided into the correlated (d) and the remainder (r) parts. The two subspaces are orthogonal. The total polarization is $\hat{P} = \hat{P}_d + \hat{P}_r$, where P_d contains $d \to d$ transitions only, while $\hat{P}_r$ accounts for $d \to r$, $r \to d$ and $r \to r$ transitions. The fundamental equations of the cRPA formalism [19] are (dropping the frequency dependence) $\hat{W} = (1 - \hat{W}_r\hat{P}_d)^{-1}\hat{W}_r$ and $\hat{W}_r = (1 - \hat{v}\hat{P}_r)^{-1}\hat{v}$, where $\hat{v}$, $\hat{W}_r$ and $\hat{W}$ are the bare, effective and fully-screened Coulomb interactions, respectively. The spherical average of the static limit of $\hat{W}_r$ is the sought-for Hubbard U parameter. The use of MLWFs basis to isolate the localized states belonging to the d subspace is commonplace and there are different methods to uncouple the r and d subspaces [23]. Here, we use the one described in Ref. [24], which is fully basis-set independent. In it, the transitions are weighted by the probability that the initial and final states belong to the d subspace. Finally, the effective Coulomb interaction matrix elements $U_{mn,m'n'}$ are calculated for a selected subset of functions out of the whole Wannier set. In order to interpret the $U_{mn,m'n'}$ matrix elements obtained in this cRPA approach as atomic Coulomb integrals, we make sure that the MLWFs conserve, to a large extent, the initial shape of the atomic orbitals (see, for example, Figs. S7 and S8 in the SM [36]). The MLWFs are also used to calculate band structure projections and orbital occupancies.

III. RESULTS AND DISCUSSION

A. Isolated planar XO_2 chains

In this subsection, we study an ideal situation where the main substrate effects are suppressed, namely the geometry change (the here-assumed coplanarity between the X and O atoms is lost in the adsorbed geometry) and charge redistribution at the metal-oxide interface. These idealized planar chains allow us to examine the screening originated exclusively by the X-O bond formation and the one-dimensionality of the system.

All the cRPA calculations are initialized with the electronic structures obtained with $U_0 = 5.5$ eV and $J_0 = 0$. Once the first U_1 is calculated using cRPA, a new DFT + U cycle is started with this value. After 4–5 iterations, convergence is achieved for MnO_2, FeO_2, and CoO_2. The resulting U and J values for the ↑↑ spin channel, shown in Table I, lie in the 5–7 eV range and are obtained independently of the U value used in the initial iteration (this was checked by starting from $U_0 = 3.5$ and 7.5 eV). The effective parameter U plays the role of the F^0 Slater integral in the Coulomb interaction term and the effective intra-atomic exchange parameter is $J = (F^2 + F^4)/14$ in the case of a d orbital [39]. F^2 and F^4 are known to be almost insensitive to screening effects [3,45] and, in fact, we obtain the typical value $J \simeq 1$ eV in the cRPA calculations. Due to the spin dependence of the single-particle states, the Wannier functions exhibit a spin dependence, too. As a consequence, we can distinguish between the matrix elements $U^{\uparrow\uparrow}$, $U^{\uparrow\downarrow}$, and $U^{\downarrow\downarrow}$. They exhibit a spread of ≈0.5 eV about their average values for FeO_2 and MnO_2, and of ≈0.2 eV for NiO_2 and CoO_2 (see Table S5 in the SM [36]). Spreads in the J values are ⩽ 0.2 eV.

TABLE I. Converged values of U and J, averaged over the ↑↑ spin channel orbitals, for the transition metal atoms in free-standing planar and Ir-supported XO_2 (sup superscript) chains. $\tilde{U}$ are the values calculated in the shell folding approach [46]. All units in eV.

XO_2	U	J	$\tilde{U}$	XO_2/Ir	U^{sup}	J^{sup}
Ni (C1)	6.59	1.17	8.45	Ni	1.71	0.87
Ni (C2)	2.41	1.01	7.03			
Mn	6.21	1.04	6.57	Mn	3.78	0.98
Co	5.73	1.11	8.62	Co	2.39	0.90
Fe	7.67	1.13	9.06	Fe	1.38	0.80

The case for NiO_2 deserves further attention. Unlike in the other chains, two electronic configurations of the Ni(d) orbital are stabilized in the initial run for different U_0 values, labelled C1 and C2 hereafter. The C1 and C2 configurations are preserved throughout the subsequent cRPA cycles, which converge to two different U values (see Table I). DFT + U calculations with $U_0 < 4$ eV yield C2 as the most stable configuration and finally $U = 2.41$ eV, while C1 is the preferred configuration for $U_0 \geqslant 4$ eV, leading to $U = 6.59$ eV. The details of d-orbital occupancies that define C1 and C2 are gathered in Table S4 in the SM [36] for the DFT + U calculations at the converged U values. Occupancies are calculated as integrals of the projected densities of states (PDOS) on the individual d-like MLWFs (see Fig. S3 in the SM [36]). The projected band structure is shown in Fig. 2.

The Ni spin moments obtained for the C1 and C2 configurations, 1.23 and 0.55 μ_B, respectively, deviate from an integer value. The closest integer is 1 μ_B in both cases, which leads us to interpret C1 and C2 to be two Ni multiplets of the same *nominal* spin state $S = 1/2$. The bare Coulomb parameters in the C1 and C2 configurations take essentially similar values, differences between individual matrix elements being, on average, 8%. This small difference in the bare Coulomb matrix is solely due to differences in the Wannier functions shape. Indeed, their real-space representations show marginal differences (see Fig. S7 in the SM [36]). Therefore, the Wannier functions shape cannot be responsible for the different U values found for C1 and C2. Instead, the origin must be in the electronic configurations adopted by Ni(d) upon the formation of the oxide chain. To confirm this interpretation, we have analyzed the bare and screened Coulomb matrix

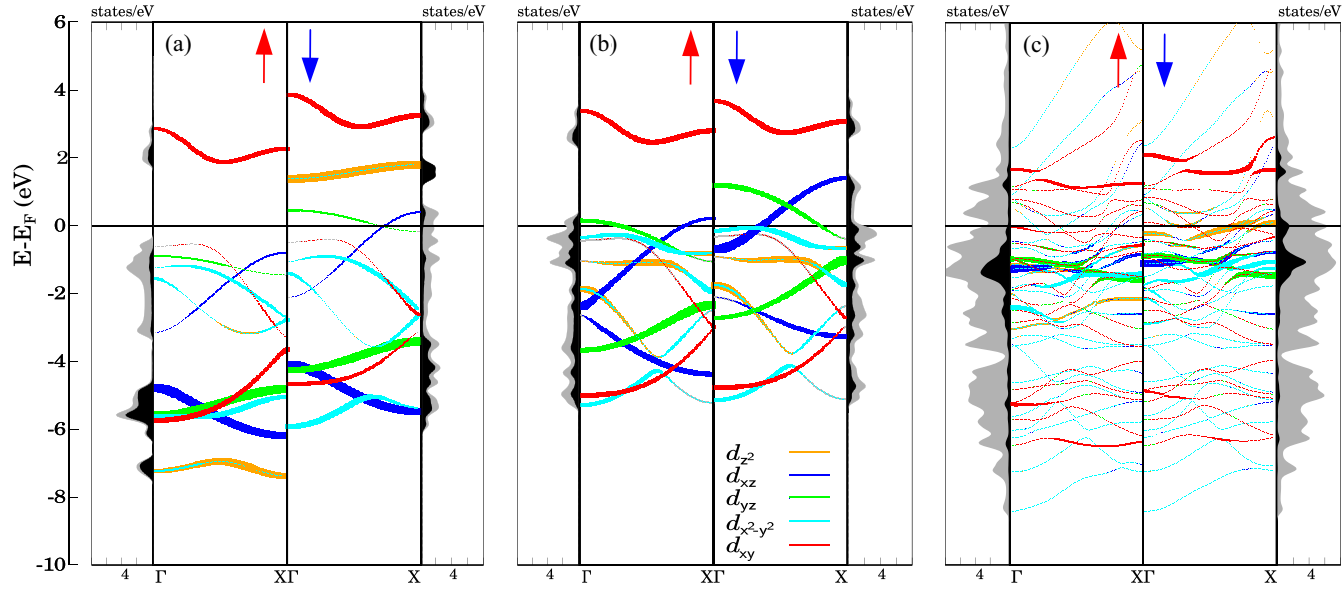

FIG. 2. Band structures (central subpanels) and densities of states (lateral subpanels) for NiO_2 chains, free standing in the C1 (a) and C2 (b) configurations, and supported on Ir(100) (c). Spin majority and minority contributions are indicated by red and blue arrows, respectively. The color code indicates the Ni(d) orbital resolved bands, obtained from projection on the corresponding MLWFs, with dot sizes accounting for the magnitude of the projection (the full bands are shown for the isolated chains, while only the projected bands on Ni(d) are shown for the supported ones). The solid gray and black shaded curves are the total and Ni(d)-projected densities of states, respectively, in each system.

elements obtained in cRPA calculations with different choices of the constrained subspace. The ↑↑ spin channel values of the elements needed in the determination of U, i.e., $U_{mn,mn}$, are summarized graphically in Fig. 3 with the contracted index notation U_{mn}. Using as baseline wavefunctions those of the C1 and C2 states at the previously converged U values [panels (a) and (d)], the new U_{mn} have been calculated with subspaces that include also the O(s) [panels (b) and (e)] and O(p) orbitals [panels (c) and (f)]. This means that in panels (a) and (d) the screening is (predominantly) due to O(sp), in panels (b) and (e) to O(p) and in panels (c) and (f) only to O(s). As a reference, the bare Coulomb matrix elements are shown in panel (g). The general trend is that the formation of Ni-O bonds largely screens the atomic Coulomb interaction at the Ni(d) orbital, reducing it from values ∼25 to ∼6.5 eV in C1 and to ∼2.5 eV in C2. The comparison of data columns (a) versus (b) and (d) versus (e) in Fig. 3 shows that, for both configurations, the screening contribution of the O(p) electrons apparently suffices to reproduce the complete screening. This does not mean that there is no significant O(s) contribution, though. In panels (c) and (f) we see that the U value for d electrons, calculated as the average $\langle \hat{U}^{dd} \rangle$ of the matrix block elements with indices $m, n = 1 - 5$, is screened by O(s) electrons from 25 to 15 eV and to 10 eV in C1 and C2, respectively. We draw two conclusions from this result: (i) The Coulomb screening of s and p channels on Ni(d) is not additive and (ii) the p screening is felt differently in C1 and C2 because each multiplet binds differently to the neighboring O atoms.

The main contribution to the screening is expected from states near the Fermi level, as they provide small denominators in the polarization expression. Therefore, in a coarse approximation, we can relate insulating and metallic behavior to weak and strong screening, respectively. Unlike in C2, in

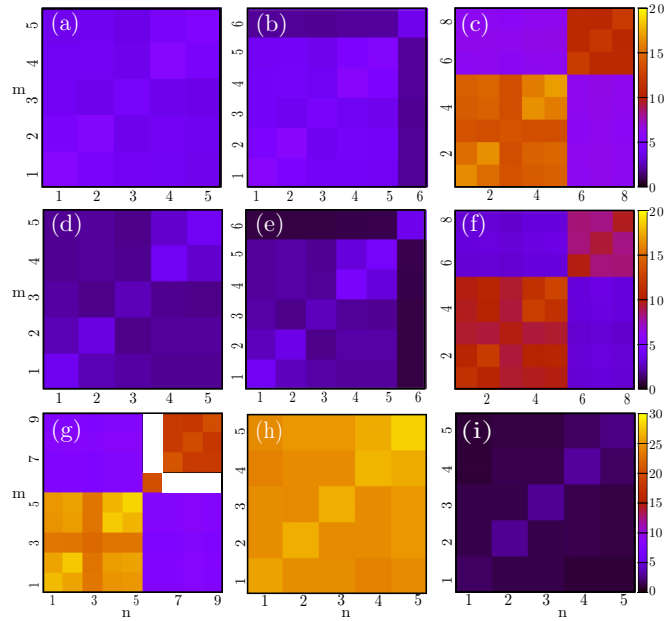

FIG. 3. Screened Coulomb matrix elements U_{mn} (↑↑ spin channel) in eV for the NiO_2 chain for selected orbitals screened by the remaining electrons. For the free-standing C1 configuration, the selection is: (a) d (indices ordered as $1 - d_{z^2}$, $2 - d_{xz}$, $3 - d_{yz}$, $4 - d_{x^2-y^2}$, and $5 - d_{xy}$), (b) d and O(s) (index 6), and (c) d and O(p) orbitals (indices ordered as $6 - p_z$, $7 - p_x$ and $8 - p_y$). [(d)–(f)] shows the same information as [(a)–(c)] but for the free-standing C2 configuration. In the bottom row, bare Coulomb matrix elements of (g) free-standing C1 and (h) Ir-supported NiO_2, which we take as reference values. (i) For Ir-supported NiO_2, U_{mn} elements of the d orbital screened by the rest of electrons. Note the different color scale for the panels (g) to (i).

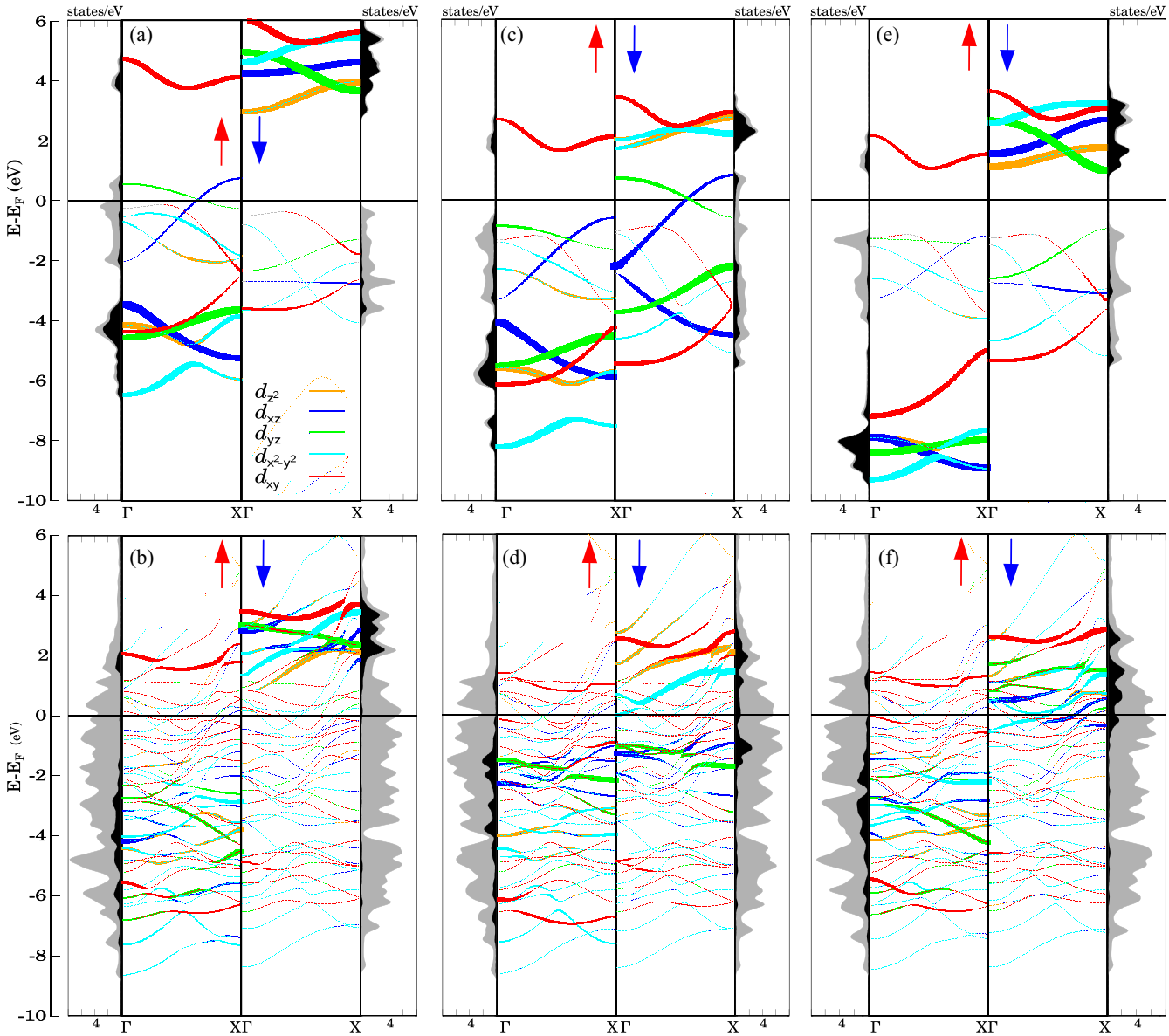

FIG. 4. The same information as in Fig. 2 is provided here for free-standing planar (top panels) and supported (bottom panels) XO_2 chains with X = Mn [(a), (b)], Co [(c), (d)], and Fe [(e), (f)].

the C1 configuration the Fermi level lies in a spin-majority bandgap, i.e., C1 is a half-metal, which is consistent with a larger effective U value (note also that the ZSA theory allows for noninsulating behavior despite U being large [1]). This qualitative DOS difference is also manifested in the spin dependence of the interaction screening: the U parameters of metallic C2 show an almost negligible spin dependence, in contrast to the other half-metallic and insulating chains (see the comparison in Table S5 in the SM [36]). As shown in Figs. 2(b) and 2(c), the main difference between the two configurations is in the hybrid d_{z^2,x^2-y^2} band [47], which is partially filled and strongly hybridized with the O(p) in C1, while it is fully filled and localized in C2. This relates to the aforementioned conclusion point (ii) in the interpretation of the screening channels. Indeed, the bindings to the ligand differ qualitatively: The sharp peaks in the DOS around $E_F - 1$ eV form a $d - d$ gap for C2, in contrast to the $d - p$ gap of C1 (see Fig. 2 and Fig. S3 in the SM [36]), which suggests that the C2 configuration is prone to undergo a Mott transition [1]. Nevertheless, from these calculations it is not possible to tell which configuration is more stable, as the DFT + U total energies obtained with different U values cannot be directly compared [48].

The results of Table I follow the trend laid down by the DOS at the Fermi level, shown in Fig. 4 and Fig. S4 in the SM [36] for the other studied isolated chains: FeO_2 is insulating (its band structure shows the features of a conventional CT insulator) and, thus, screening is the weakest ($U = 7.67$ eV) among the different studied systems, while it is somewhat stronger in the half-metallic systems MnO_2, CoO_2, and NiO_2-C1 (with U values close to 6 eV), and even stronger in metallic NiO_2-C2 ($U = 2.41$ eV). In Ref. [49] an expression of the screened U is given as the derivative of the Kohn-Sham

potential with respect to the number n_d of electrons in the d orbital, which makes clear the explicit dependence on the relaxation of the d bands themselves for a given occupancy. When this expression is applied to the case of TM impurities of the same valence state embedded in an alkali metal (Rb), screening increases linearly with n_d, and it is stronger for monovalent than for divalent impurities. In the four XO_2 isolated chains this scaling does not apply, because of the more complex chemical environment, involving directional bonds and orbital-specific band dispersion. Indeed, while the d-shell occupancies are similar in the C1 and C2 configurations [$n_d(\mathrm{C1}) = 7.71$ and $n_d(\mathrm{C2}) = 7.92$], the U parameters are clearly different (Table I), due to the pronounced screening contribution from s and p electrons.

It has been argued in Ref. [46] that considering a correlated subspace of d states in a system as the present chains, where the TM d orbitals strongly hybridize with the O(p) ligands, often leads to an underestimation of the U values. In these chains, a bonding-antibonding $d_{xy} - p_{x,y}$ pair is formed, which appears as a one-dimensional dispersive occupied band of width ∼2 eV (see red data points in Figs. 2 and 4). It is also manifested in the MLWF corresponding to the d_{xy} orbital, which acquires a nodal feature between the atoms (see the NiO_2 and FeO_2 cases in Figs. S7 and S8, respectively, in the SM [36]). In principle, by having this localized wavefunction in the correlated space for cRPA, the splitting between the X(d) space and the rest space (r) retains a partial contribution of the O(p) ligands in the correlated subspace [23]. Alternatively, when using a correlated subspace formed by p and d electrons, like in Figs. 3(c) and 3(f), the off-diagonal 5×3 matrix blocks $\hat{U}^{dp}$ account for *intershell* interactions that renormalize the *intrashell* interaction matrix blocks $\hat{U}^{dd}$ and $\hat{U}^{pp}$. This is the so-called "shell folding" approach [46], whereby, if the total occupation of the d and p subspaces remains invariant under changes in U, the renormalized average interaction between the d electrons is written simply as $\tilde{U} \equiv \langle \hat{U}^{dd} \rangle - \langle \hat{U}^{dp} \rangle$. This expression corrects the contribution of itinerant electrons to screening. With this approach we obtain $\tilde{U} > U$ (see Table I and further details in Table S6 and Figs. S6 in the SM [36]). In the case of MnO_2 the difference is only 0.36 eV, which means that the ligand is almost fully disentangled from the correlated d subspace [Figs. 5(a) and 5(b) show the U_{mn} matrix elements], while for NiO_2-C2 the difference is as large as 4.62 eV. Moreover, we find an average $\langle \hat{U}^{dp} \rangle = 3.28$ eV in NiO_2-C2, while it is ∼6 eV for the other four cases. NiO_2-C2 also has a lower $\langle \hat{U}^{dd} \rangle$ (see Table S6 in the SM [36]). We recall that this case is characterized by a $d - d$ type gap, while the others follow a $p - d$ gap behavior, where bands of predominant p character appear separated [see Fig. 2(a) and Figs. 4(a), 4(c), and 4(e)]. This is consistent with the lower values of $\langle \hat{U}^{dp} \rangle$ and $\langle \hat{U}^{dd} \rangle$ in NiO_2-C2. Therefore, the intershell interactions in the C2 configuration are qualitatively different from the other studied cases.

B. XO_2/Ir(100)-1 × 3

For oxide films on a metal, the Coulomb interaction can be modelled as the difference between the ionization and affinity energies, each corrected by the image potential energy

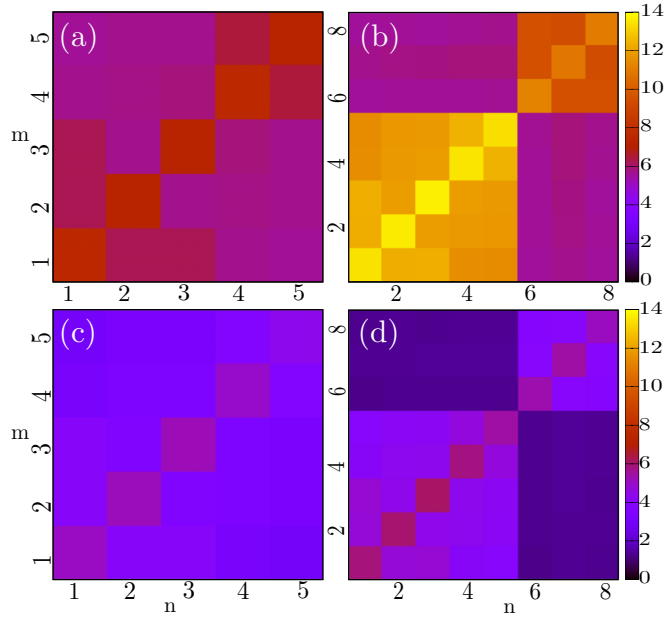

FIG. 5. Effective U_{mn} Coulomb matrix elements (in eV) in the isolated MnO_2 chain including (a) only Mn(d) electrons and (b) Mn(d) and O(p) electrons in the correlated subspace. Panels [(c), (d)]: same quantities for the supported MnO_2 chain. [Note, O(s) electrons, which belong to the correlated space in panel (d), are not shown.]

E_{im} created by the charged X(d) shell [2,3], $U = E(d^{n-1}) + E(d^{n+1}) - 2E(d^n) - 2E_{im}$, where each total energy term is calculated for a fixed population of the d orbital. When the XO_2 chains are adsorbed on the Ir(100) substrate there is, indeed, a reduction in the screened U values with respect to the planar free-standing chains in the range $0.7 - 6.3$ eV, being strongest for FeO_2. These results, obtained after 3–4 convergence cycles with cRPA, are shown in Table I. Hybridization between chain orbitals and Ir states, clearly visible in the band structures, results in a nonuniform charge redistribution at the interface. The reduction of the intraatomic Coulomb interaction in X(d) will depend on the interfacial electronic structure details, which can be captured by *ab initio* methods, but not by an image charge model potential [50]. Charge transfer upon adsorption modifies the X(d) orbital occupancies, eventually forcing it to adopt a very different multiplet configuration from that of the isolated case. As we have seen in the previous section, this can have a dramatic effect on the screening contribution of the p ligands. In brief, the overall screening observed upon adsorption may have a non-negligible indirect contribution from a multiplet change. The importance of this additional mechanism depends on the chain composition. We note in passing that the noncoplanar atomic geometry adopted on the Ir(100) substrate alters the band structure of the chains, but this does not suffice to produce significant variations in the U, J values with respect to the planar geometry (we have checked that the U values obtained by cRPA for buckled MnO_2 free-standing chains, where the atomic positions are set as in the adsorbed geometry, are not significantly affected by this distortion, although it does change the bands dispersion, as shown in Fig. S2 in the SM [36]).

The particular case of MnO_2/Ir(100) allows us, as we discuss next, to obtain a separate estimation of the contribution of the metal substrate effect from that of the ligand effect. We recall that in the isolated MnO_2 chain the $U - \tilde{U}$ difference was small, which we interpreted as a nearly full disentanglement of the d space from the ligand in the calculation of $U = 6.21$ eV. This value drops to $U^{\text{sup}} = 3.78$ eV for the adsorbed chain (we use the superscript sup in the following to denote the U values of the supported chains). Figure 4 top panels show that the MnO_2 band structure undergoes significant changes due to hybridization with Ir, yet, the changes in the Mn(d) orbital occupations (Table S4 in the SM [36]) are subtle. Alternatively, we can consider a correlated subspace formed by Mn(d) and O(p) and apply shell folding renormalization to the matrix elements shown in Fig. 5(d). We obtain $\tilde{U}^{\text{sup}} \equiv \langle \hat{U}^{dd,\text{sup}} \rangle - \langle \hat{U}^{pd,\text{sup}} \rangle = 3.29$ eV, which is close to the value obtained in the usual calculation, $U^{\text{sup}} = 3.78$ eV. This implies that, as in the isolated case, the ligand orbitals in MnO_2/Ir(100) are well disentangled and we can estimate the separate Ir contribution to the interaction as the difference $\langle \hat{U}^{dd,\text{sup}} \rangle - U^{\text{sup}} = 0.88$ eV or as $\langle \hat{U}^{dd,\text{sup}} \rangle - \tilde{U}^{\text{sup}} = 1.37$ eV. Therefore, in the reduction from U to U^{sup} (Table I), generally $\simeq$1 eV can be attributed to the hybridization with Ir.

Next, we consider the NiO_2 chains. In the adsorbed state, the Ni(d) configuration resembles better that of C2 than C1 (see Table S4 in the SM [36] and Fig. 3). Since the C1 configuration is not found on the surface (not even as a metastable state), we interpret this fact as a consequence of the multiplet effect playing a dominant role in the screening of Coulomb interactions in NiO_2/Ir(100), leading to the low value $U^{\text{sup}} = 1.71$ eV (calculated for the $\uparrow\uparrow$ channel). Indeed, to probe the robustness of the result on Ir, we have initialized the cRPA iterations with high and low U_0 values and Ni(d) frozen C1 and C2 configurations. In all cases, the calculation converges towards the U^{sup} values and occupancies shown in Table I and Table S4 in the SM [36]. Ni(d) states remain overall as narrow bands around the Fermi level. In particular, the hybrid d_{z^2,x^2-y^2} states, which form an anticrossed pair of narrow bands at $E_F - 1$ eV in the isolated NiO_2-C2 chain [47] [cyan and orange bands close to the Fermi level in Fig. 2(b)], become partially occupied by a relatively weak hybridization with Ir states [note that the states that lie at the Fermi level have predominantly d_{z^2} character in Fig. 2(c)] and, therefore, screening is expected to be enhanced. All in all, the multiplet features that lead to the low $U = 2.41$ eV value in isolated NiO_2-C2 are present also in the NiO_2/Ir(100) adsorbed case. The further reduction to $U^{\text{sup}} = 1.71$ eV is compatible with the already mentioned hybridization mechanism, consisting of a reduction of $\simeq$1 eV, as estimated from the MnO_2/Ir(100) case. The same procedure for NiO_2/Ir(100), shown in Table S6 in the SM [36], would yield a smaller reduction of $\langle \hat{U}^{dd,\text{sup}} \rangle - U^{\text{sup}} = 0.28$ eV, probably due to the stronger entanglement with O(p) ligands detected at NiO_2-C2.

Finally, we address the FeO_2 case. A very efficient overall screening, with a dramatic reduction of the U value from 7.67 to 1.38 eV, is found in adsorbed FeO_2/Ir(100). The Fe(d) multiplet is changed by interaction with the Ir substrate, changing from a $S = 2$ to a $S = 3/2$ state (see Table S4 in the SM [36]). The FeO_2 band structure, which is that of a CT insulator when the chain is isolated, becomes conducting upon hybridization with Ir, as the Fe(d) spin-minority band bottom edge is pinned to the Fermi level. We attribute the strong U reduction of the Fe(d) shell to this insulating-to-metallic transition. The pinning of the Fe(d) spin-minority band at the Fermi level persists when high U values are used in the band structure calculation and when the FeO_2 chain is artificially lifted from the substrate. To ascertain whether the huge reduction in the U value upon adsorption is physically meaningful or is an artifact due to a residual chain states pinning at Fermi, we have lifted the chain until achieving detachment, i.e., to the height z_{Fe} where there is no charge transfer from the substrate and screening is due only to the metal surface image potential. First, we have carried out cRPA for structures with intermediate height $z_{\text{Fe}} = 2.5$ Å and two initial U_0 values to prevent stagnation at metastable states. Starting from both $U_0^f = 7.67$ eV (the converged free-standing value, labeled f) and $U_0^{\text{sup}} = 1.38$ eV (the converged supported value), the value is stabilized at $\simeq$3.5 eV after two iterations and a residual peak of chain states is still visible at the Fermi level. A height as large as $z_{\text{Fe}} = 4$ Å is needed for these residual states to vanish, as shown in Fig. S5(d) in the SM [36] (the PDOS corresponding to some of those cases is shown in Fig. S5 in the SM [36]). However, at this distance, the U parameter does not stabilize at the value of the free-standing chain U_0^f, but reduces to 6.13 eV after one iteration. Starting from the adsorbed value U_0^{sup}, it results in 3.81 eV. Therefore, despite the hybridization of the chain states with the surface is negligible at $z_{\text{Fe}} = 4$ Å, a non-negligible screening persists. This behavior is not necessarily unphysical: It means that the calculation accounts for the substrate potential tail, at least partially. Nevertheless, in order to accurately describe the screening for far-lying chains, a different exchange and correlation (xc) functional would be needed. Note, the GGA, being a semilocal xc functional, works by error cancellation, providing a poorer description when low electron densities are involved in the interactions, failing to provide an accurate asymptotic $1/z$ behavior.

IV. CONCLUSIONS

In summary, we have performed a cRPA investigation of magnetic one-dimensional transition metal oxide XO_2 chains deposited on a Ir(100) surface aimed at understanding the screening of intraorbital Coulomb interactions in the X(d) shell under the combined effect of low dimensionality, the ligand field and a neighboring metal.

Calculations for the isolated XO_2 chains show a strong dependence of the Hubbard U parameter on the X species, ranging from 2.4 to 7.7 eV. In each case, the U value reflects the insulating or (half)metallic character of the chain. Importantly, we find low-U and high-U regimes in the case of NiO_2 associated to $d - d$ (Mott-Hubbard) or $p - d$ (charge transfer) gap types, respectively. The gap type is determined by the Ni(d) electronic configuration or multiplet. In the particular case of NiO_2, multiplets with even the same orbital filling and same spin state (as it is the case of the C1 and C2 multiplets found in the present work) lead to different regimes. Due to the interaction with the O(p) ligands, the inclusion of O(p)

electrons in the cRPA correlated subspace results in a different renormalization and higher values of the U parameter for each transition-metal species. The increase is smallest for MnO_2 and largest for the NiO_2 in the Mott-Hubbard-like multiplet.

Since the ligand field is weak for MnO_2, this case allows us to establish that the U reduction by interaction with the metallic substrate is $\simeq$1 eV and a much larger reduction comes from the change of the occupation of the d states. In general, however, the contributions of substrate and ligand cannot be uncoupled. Adsorption drives the formation of interfacial states and charge transfer to the chain, which in turn can undergo an insulator-to-metal transition (such is the FeO_2 case, where the value of U is reduced by almost 6 eV) or have its multiplet configuration altered. The latter is the scenario for NiO_2/Ir(100), where a low value of 1.71 eV is obtained in part because the substrate adopts the Mott-Hubbard-like multiplet. Incidentally, the fine details of the band dispersion play a lesser role in the determination of the U parameter.

All in all, Coulomb interactions in a low-dimensional oxide by a neighboring metal cannot be described in simple terms by a charge screening model. Instead, the fine details of the hybrid oxide-metal electronic structure must be considered, as they also affect the renormalization of the interactions due to the O(p) ligands.

ACKNOWLEDGMENTS

Projects No. PID2019-103910GB-I00 funded by MCIN/AEI, 10.13039/501100011033/; No. GIU18/138 by Universidad del País Vasco UPV/EHU; No. IT-1246-19 and No. IT-1260-19 by Gobierno Vasco. Computational resources were partially provided by the DIPC computing center. S.B. acknowledges funding from the Deutsche Forschungsgemeinschaft (DFG) through priority program SPP 2137 "Skyrmionics" (Project No. BL 444/16) and the Collaborative Research Centers SFB 1238 (Project No. C01).

[1] J. Zaanen, G. A. Sawatzky, and J. W. Allen, Phys. Rev. Lett. **55**, 418 (1985).
[2] D. M. Duffy and A. M. Stoneham, J. Phys. C **16**, 4087 (1983).
[3] S. Altieri, L. H. Tjeng, F. C. Voogt, T. Hibma, and G. A. Sawatzky, Phys. Rev. B **59**, R2517 (1999).
[4] J. van den Brink and G. A. Sawatzky, Europhys. Lett. **50**, 447 (2000).
[5] L. Peters, E. Şaşıoğlu, S. Rossen, C. Friedrich, S. Blügel, and M. I. Katsnelson, Phys. Rev. B **95**, 155119 (2017).
[6] V. I. Anisimov, F. Aryasetiawan, and A. I. Lichtenstein, J. Phys.: Condens. Matter **9**, 767 (1997).
[7] A. I. Liechtenstein, V. I. Anisimov, and J. Zaanen, Phys. Rev. B **52**, R5467 (1995).
[8] A. I. Lichtenstein and M. I. Katsnelson, Phys. Rev. B **57**, 6884 (1998).
[9] L. Hedin, Phys. Rev. **139**, A796 (1965).
[10] C. Møller and M. S. Plesset, Phys. Rev. **46**, 618 (1934).
[11] D. Langreth and J. Perdew, Solid State Commun. **17**, 1425 (1975).
[12] G. Kotliar, S. Y. Savrasov, K. Haule, V. S. Oudovenko, O. Parcollet, and C. A. Marianetti, Rev. Mod. Phys. **78**, 865 (2006).
[13] S. Biermann, J. Phys.: Condens. Matter **26**, 173202 (2014).
[14] S. Biermann, F. Aryasetiawan, and A. Georges, Phys. Rev. Lett. **90**, 086402 (2003).
[15] P. H. Dederichs, S. Blügel, R. Zeller, and H. Akai, Phys. Rev. Lett. **53**, 2512 (1984).
[16] M. Cococcioni and S. de Gironcoli, Phys. Rev. B **71**, 035105 (2005).
[17] I. Timrov, N. Marzari, and M. Cococcioni, Phys. Rev. B **98**, 085127 (2018).
[18] I. Timrov, N. Marzari, and M. Cococcioni, Phys. Rev. B **103**, 045141 (2021).
[19] F. Aryasetiawan, M. Imada, A. Georges, G. Kotliar, S. Biermann, and A. I. Lichtenstein, Phys. Rev. B **70**, 195104 (2004).
[20] F. Aryasetiawan, K. Karlsson, O. Jepsen, and U. Schönberger, Phys. Rev. B **74**, 125106 (2006).
[21] G. Pizzi, V. Vitale, R. Arita, S. Blügel, F. Freimuth, G. Géranton, M. Gibertini, D. Gresch, C. Johnson, T. Koretsune *et al.*, J. Phys.: Condens. Matter **32**, 165902 (2020).
[22] N. Marzari and D. Vanderbilt, Phys. Rev. B **56**, 12847 (1997).
[23] T. Miyake, F. Aryasetiawan, and M. Imada, Phys. Rev. B **80**, 155134 (2009).
[24] E. Şaşı oğlu, C. Friedrich, and S. Blügel, Phys. Rev. B **83**, 121101 (2011).
[25] P. Ferstl, L. Hammer, C. Sobel, M. Gubo, K. Heinz, M. A. Schneider, F. Mittendorfer, and J. Redinger, Phys. Rev. Lett. **117**, 046101 (2016).
[26] P. Ferstl, F. Mittendorfer, J. Redinger, M. A. Schneider, and L. Hammer, Phys. Rev. B **96**, 085407 (2017).
[27] M. Schmitt, C. H. Park, P. Weber, A. Jäger, J. Kemmer, M. Vogt, and M. Bode, Phys. Rev. B **100**, 054431 (2019).
[28] J. G. Korobova, I. A. Nikitina, D. I. Bazhanov, and P. Ruiz-Díaz, J. Phys. Chem. C **124**, 26026 (2020).
[29] M. Schmitt, P. Moras, G. Bihlmayer, R. Cotsakis, M. Vogt, J. Kemmer, A. Belabbes, P. M. Sheverdyaeva, A. K. Kundu, C. Carbone *et al.*, Nat. Commun. **10**, 2610 (2019).
[30] S. G. Altendorf, A. Reisner, B. Tam, F. Meneghin, S. Wirth, and L. H. Tjeng, Phys. Rev. B **97**, 165422 (2018).
[31] S. Barman, A. K. Kundu, and K. S. Menon, J. Magn. Magn. Mater. **515**, 167292 (2020).
[32] J. B. Goodenough, Phys. Rev. **100**, 564 (1955).
[33] J. Kanamori, J. Phys. Chem. Solids **10**, 87 (1959).
[34] G. Kresse and J. Hafner, Phys. Rev. B **47**, 558 (1993).
[35] G. Kresse and D. Joubert, Phys. Rev. B **59**, 1758 (1999).
[36] See Supplemental Material at http://link.aps.org/supplemental/10.1103/PhysRevB.106.035130 for further details on the calculation parameters, spin-dependent U and J values, and electronic structure.

[37] Inclusion of a third Ir layer in a cRPA iteration changes the obtained U value for MnO_2/Ir by ∼10%.

[38] J. P. Perdew, K. Burke, and M. Ernzerhof, Phys. Rev. Lett. **77**, 3865 (1996).

[39] V. I. Anisimov, I. V. Solovyev, M. A. Korotin, M. T. Czyżyk, and G. A. Sawatzky, Phys. Rev. B **48**, 16929 (1993).

[40] FLEUR site: http://www.flapw.de

[41] H. Krakauer, M. Posternak, and A. J. Freeman, Phys. Rev. B **19**, 1706 (1979).

[42] E. Wimmer, H. Krakauer, M. Weinert, and A. J. Freeman, Phys. Rev. B **24**, 864 (1981).

[43] A. B. Shick, A. I. Liechtenstein, and W. E. Pickett, Phys. Rev. B **60**, 10763 (1999).

[44] C. Friedrich, S. Blügel, and A. Schindlmayr, Phys. Rev. B **81**, 125102 (2010).

[45] D. van der Marel and G. A. Sawatzky, Phys. Rev. B **37**, 10674 (1988).

[46] P. Seth, P. Hansmann, A. van Roekeghem, L. Vaugier, and S. Biermann, Phys. Rev. Lett. **119**, 056401 (2017).

[47] Due to the chain symmetry, bands stemming from d_z^2 and $d_{x^2-y^2}$ atomic orbitals hybridize. In fact, as shown in Fig. 2, anti-crossing features appear for bands with weight in the MLWFs corresponding to d_z^2 and $d_{x^2-y^2}$, while not on bands with d_{xz}, d_{yz}, or d_{xy} character, as the latter belong to different symmetry representations.

[48] Since in DFT + U the Hubbard terms are applied to a subset of Kohn-Sham eigenstates, which have no physical meaning on their own, only total energies obtained in same-U calculations can be compared. For the particular values $U = 6$ and $J = 1$ eV for Ni(d), we find that C2 is metastable with an energy difference of 0.33 eV with respect to C1.

[49] I. V. Solovyev and P. H. Dederichs, Phys. Rev. B **49**, 6736 (1994).

[50] The image potential tail behaves as $-q/4(z - z_X)$, where q is the X(d) charge, z_X is the X atom adsorption height and z the vertical distance from the surface. However, the X atom is too close to the surface for that law to be applicable, since it is partially inserted in the trough of the Ir missing row (z_X values lie in the 0.7–1.25 Å range [25]).